International Journal of Climatology

International Journal of Climatology RMetS

RESEARCH ARTICLE

Simple GCM Simulations of Rainfall Over Northeast Brazil, Part 2: Model Performance for Historical Seasonal Forecasts

Francisco das Chagas Vasconcelos Junior[1] | Nicholas M. J. Hall[2] | Leticia Cardoso[1] | Aubains Hounsou-Gbo[3] | Eduardo S. P. R. Martins[1,3]

[1]Ceará Institute for Meteorology and Water Resources–Funceme, Fortaleza, Brazil | [2]University of Toulouse–LEGOS–IRD/UT3/CNRS/CNES, Toulouse, France | [3]Universidade Federal do Ceará–LABOMAR, Fortaleza, Brazil

Correspondence: Francisco das Chagas Vasconcelos Junior (francisco.vasconcelos@funceme.br)

Received: 5 January 2024 | **Revised:** 28 October 2024 | **Accepted:** 6 December 2024

Funding: This work was supported by Conselho Nacional de Desenvolvimento Científico e Tecnológico. Institut de Recherche pour le Développement.

ABSTRACT

A dynamical model is used as a simple GCM to perform historical forecasts for rainfall in northeastern Brazil for the years 1982–2020. The model is forced by empirically derived source terms and includes basic parameterisations to simulate vertical diffusion, convection and condensation. Ensemble forecasts with 38 members are initiated on 1st January using persisted tropical sea surface temperature anomalies (SSTAs). Rainfall forecast performance is evaluated for the February–April (FMA) rainy season. The model reproduces the climatological precipitation in the specified Nordeste region with a mainly dry bias as the model rainfall maximum is displaced in the the northwest. Hindcasts for interannual rainfall anomalies correlate with observed values ($r = 0.46$) and model variance is weaker than observed. A further set of forecast experiments with SSTAs restricted to the three major ocean basins reveals that most of the forecast skill can be attributed to the Pacific, despite the model's greater sensitivity to Atlantic SSTAs. The sum of results from the three ocean basins is close to the full hindcast result. Finally, a set of 128 forecast runs with idealised SSTAs placed regularly within the tropics is carried out to calibrate the response of modelled rainfall to remote influences. An influence function is diagnosed in the form of a tropical distribution of northeastern Brazil rainfall in mm/day per unit SSTA. It is strongly concentrated in the tropical Atlantic, with dry/wet conditions resulting from positive SSTAs in the northern/southern tropical Atlantic, in keeping with the observed covariance. The influence function is the used to construct a linear approximation to the forecast performance of the simple GCM. It has similar skill but stronger variance, and the skill is partitioned differently between Atlantic and Pacific influences.

1 | Introduction

Signals propagate though the atmosphere on a global scale within a few days. For this reason, physically based seasonal prediction of regional continental rainfall must involve the global atmosphere. But atmospheric dynamics is intrinsically unpredictable beyond a couple of weeks. So successful prediction past this limit relies on predictable elements of the system that are able influence the global atmosphere on longer time scales. This is the vision of extended predictability described by Hoskins (2013) and Robertson and Vitart (2018). The potentially predictable components that can contribute to subseasonal to seasonal (S2S) variations of rainfall over the Nordeste region of Brazil are in increasing order of timescale: the Madden-Julian Oscillation (MJO, Vasconcelos Junior et al. 2021); continental soil moisture (Dirmeyer and Halder 2017) and global Sea Surface Temperatures (SSTs).

Moron and Robertson (2020) show that SST anomalies (SSTAs) present a source of S2S potential predictability for tropical rainfall. Predictability is better over the tropical oceans than over the continent, as large-scale convective rainfall prevails over

the oceans and SSTs evolve slowly, whereas the scale of continental rainfall anomalies tends to be smaller and they respond to a range of influences (Uvo et al. 1998; Folland et al. 2001; Misra 2006; Doblas-Reyes et al. 2013). Predictability improves when teleconnections between oceanic SSTA responses are well simulated (Scaife et al. 2019), and such teleconnections may in turn augment continental predictability. A global simulation is therefore necessary if one seeks to make physically based forecasts that depend on the link between SSTAs and continental rainfall.

Improved observational data and advances in our understanding of climate processes, modelling techniques and computing power have driven significant evolution in seasonal forecasting systems over the last few decades. Improvements have also come from combining global climate models and calibrating their results to build systems focused on applications such as water resources, agriculture and power planning (Eade et al. 2014; Shukla et al. 2014; Tompkins et al. 2017; Basso and Liu 2019; Delgado et al. 2018; Pilz et al. 2019). In 1999, the International Climate Institute from Columbia University developed first Seasonal Climate Forecast System with three models and different SST boundary conditions (Mason et al. 1999), and in 2006, the World Meteorological Organisation (WMO) initiated a collaborative multi-model system involving several global centres for long-range forecasts, with standard sets of forecasts products and a WMO-defined verification process for retrospective forecasts. In 2011, the North American Multi-Model Ensemble (NMME) was launched involving collaboration between several institutes in the US and Canada to produce an operational prediction system focused on decision support for a wide range of users who rely on climate information (Kirtman et al. 2014). The European initiative from the Copernicus Climate Change Service, implemented by the ECMWF, started a Multi-System Forecasts in 2018, which comprises operational model results from Météo-France, the German Weather Service, the Euro-Mediterranean Center on Climate Change, the UK Met Office, the ECWMF and NCEP.

Progress has also been made by allowing the boundary conditions to evolve during the forecast. For example, various approaches to ENSO prediction (Ropelewski and Halpert 1987; Barnett and Preisendorfer 1987; Barnston et al. 2003) have benefited forecasts in extratropical Pacific North America (Barnett et al. 1993), and seasonal rainfall predictability in the tropics (Ward and Folland 1991; Hastenrath 2012). Further progress in physically based forecasts is documented by Balmaseda, Anderson, and Davey (1994). Important developments followed the implementation of coupled ocean–atmosphere models and ensemble techniques, enabling a probabilistic approach, quantifying uncertainties and improving the forecast reliability (Barnston et al. 2003; Hagedorn, Doblas-Reyes, and Palmer 2005; Doblas-Reyes et al. 2013; Li et al. 2009; Kirtman and Pirani 2009). These advances have enabled the development of more sophisticated and reliable climate models, facilitating more accurate and useful seasonal forecasting for a variety of sectors.

At FUNCEME in the state of Céara, seasonal forecasts are issued at the beginning of January for the February–April (FMA) Nordeste rainy season using the ECHAM General Circulation Model version 4 (T42 horizontal resolution, 19 vertical levels, Roeckner et al. 1996; Stevens et al. 2013), which has been in use since 2011 (Canamary, Reis Jr, and Martins 2015) and more recently it was offline coupled to a hydrological model to evaluate water allocation process in a semiarid region (Pereira et al. 2023). Interannual variability of Nordeste rainfall is exceptionally strong and the region has seen a sequence of droughts and extreme precipitation from 1 year to the next, with severe consequences for agriculture, water resources and power generation. Seasonal rainfall forecasts are therefore of great importance for the region. Current forecasts of the FMA season with a lead time of 1 month depend on the notion that persisted SSTAs can furnish the required predictability. There is a long history in the literature of linking SSTAs with Nordeste rainfall variability. El Niño and Tropical Atlantic variability are known drivers (see e.g., Cai et al. 2020; Coelho et al. 2021; Hastenrath 2012). It should be noted, however, that the use of persisted SSTAs may be of limited general applicability. Situations where long-lived SSTA patterns such as El Niño have a dominant impact on forecasts, particularly for the southern summer rainy season, are likely to represent a best-case scenario for forecast skill with persisted SSTAs.

The modelling study presented in this article can in no way compete with the resources and institutional collaborations described earlier. We present a set of forecasts with an idealised model in a simplified experimental framework. This provides a complement to the activity of national and international prediction centres, for more academic questions which would potentially entail prohibitive costs if they were to be investigated with a fully specified GCM. If successful, such a stripped-down forecast system might also be useful for institutions that have limited computer resources. The simple GCM used in this study is a global dynamical model called Dynamical Research Empirical Atmospheric Model (DREAM, Hall, Leroux, and Ambrizzi 2019; Hall and Leroux 2023). It is driven by an empirically derived, seasonally varying source term that is added to the primitive equations. This source term is derived from a reanalysis climatology, and by forcing the model this way many of the expensive physical parameterisations that are included in fully specified GCMs can be bypassed. The only processes that are parameterised are the ones that are essential to complete the chain of causality from an SSTA to continental rainfall. It should be noted that even though the source terms that drive the model are derived from data, DREAM is a physical model and the forecasts present in this article are physically based. There is no statistical element to these forecasts.

In the companion to this article (Hounsou-Gbo et al. 2024, hereafter part 1) we describe these canonical SSTA modes and show how they impact continental rainfall in a simple GCM. Our simulations reproduce the known associations between SSTA patterns and Nordeste rainfall reasonably well. In this article we consider whether these promising responses to canonical SSTA patterns can translate into seasonal forecast skill when the model is driven by observed SSTAs.

The version of DREAM used in part 1, and in this study, includes a moisture variable, a simple vertical diffusion scheme and basic representations of convective and large-scale condensation. Even when these physical schemes are included, DREAM

runs an order of magnitude faster than ECHAM on the same computer system. This makes it an attractive proposition for a flexible forecast system, with which a large number of test simulations can be carried out. The comparison with the state of the art is even more favourable given the relatively low resolution used for both DREAM and ECHAM. The purpose of this study is to evaluate the performance of DREAM for the FMA Nordeste rainy season, over the period 1982–2020.

In section 2 we provide a description of DREAM, the datasets used and the implementation of the historical forecasts. Section 3 contains the results including a model validation for global climatological rainfall and the interannual statistics for observed and forecast Nordeste rainfall. Section 4 contains some further results in which we try to attribute forecast performance to Pacific, Atlantic and Indian Ocean SSTAs. In section 5 we present an extensive study of the response of the model, in forecast mode, to a regular grid of idealised SSTAs, culminating in an influence function for Nordeste FMA forecast rainfall. This influence function is compared with observed regression statistics, and it is then used to construct a linear model of the forecast performance of DREAM. The results are discussed in section 6.

2 | Model, Data and Experimental Design

In this section we give a brief recap of the essential aspects of DREAM relevant to this study, as a more extended description of DREAM is given in part 1. DREAM originates from the global spectral primitive equation model of Hoskins and Simmons (1975) which was first adapted by Hall (2000) to run as a simple GCM, replacing most of the physical parameterisations found in a fully specified GCM with a fixed empirical forcing term derived from a reanalysis dataset.

This empirical forcing is calculated by initialising an unforced dynamical model with a large set of initial conditions and taking the negative mean of all the initial tendencies. This provides a spatially varying time-independent multivariate field, to be used as a set of source terms for the primitive equations. These source terms act to counter the mean initial tendency that the unforced model would have, resulting in a dynamical model that can be run as a GCM. It develops a realistic mean state and temporal variability, allowing it to be used for dynamical sensitivity studies in the context of real-world climate or forecast simulations. The initial conditions used to calculate the empirical forcing are taken from 38 years of ERA-interim reanalysis (Simmons 2006) from 1979 to 2016. The version of DREAM used in this article has an annual cycle in the forcing (Hall, Leroux, and Ambrizzi 2019) and is thus capable of simulating the changing seasons throughout a seasonal forecast. The empirical forcing applied to DREAM represents sources that are treated as independent of the model state. Dissipative terms and further parameterisations that depend on the model state are included in the model. These include linear vertical diffusion and scale selective horizontal diffusion on 3-d state variables, with some additional damping to represent radiative cooling.

A basic representation of moist thermodynamics has been added, necessary to simulate rainfall. This includes a deep convection scheme that uses vertically integrated moisture flux convergence to provide both a triggering criterion and a precipitation rate within specified limits. There is a pro-rata depletion of the specific humidity in the column and the associated diabatic heating is distributed into a deep convective profile. The model has a large-scale, in situ condensation scheme to remove remaining supersaturation. In this study DREAM is run at T31 horizontal resolution with 15 vertical levels. Further details of these parameterisations are given in Part 1 and a complete guide to how DREAM works and how to use it is provided by Hall and Leroux (2023).

The empirical forcing technique was first used by Roads (1987) to assess mid-latitude predictability using an ensemble of predictions in a quasi-geostrophic model. Since that pioneering study, DREAM and its predecessors have been used several times for ensemble predictability studies (Hall, Lin, and Derome 2001; Derome, Lin, and Brunet 2005; Tang, Lin, and Moore 2008) and numerous times for more idealised ensemble studies like the one presented in part 1. In this article, and in part 1, DREAM is used for the first time with moist thermodynamics. This is also the first time that the object of study is a tropical phenomenon. Finally, it is the first time this dynamical model has been forced from the surface by SST anomalies, rather than merely perturbed by an idealised heating distribution imposed throughout the depth of the troposphere.

Boundary fluxes of heat and humidity are calculated using both the climatological SST and the departure from the climatology, in this case a persisted January SSTA. The SST data we use for these forecasts is from the NOAA/Reynolds dataset (Reynolds et al. 2002) for monthly-mean climatology (1971–2000) and weekly-mean SSTs starting in 1982. The persisted SSTA is calculated as the difference between the current week's SST at 00Z on 1 January for each forecast year and the December–February (DJF) mean SST climatology.

Ensemble forecasts are carried out with DREAM using the same initialisation and timing as in part 1. All 38 of the 00Z 1 Jan states are used as initial conditions for ensemble members and the model is run from 1 Jan to the end of April, using the FMA season for diagnostics. Thirty-nine forecasts are made with SSTAs from 1982 to 2020. The only distinction between forecasts for different years is the persisted 1 Jan SSTA.

An additional analysis arises from the consideration of data from the NMME models (Kirtman et al. 2014); in this context, we take the ensemble mean of the retrospective forecasts initialised in January for the years between 1982 and 2020.

FMA rainfall is averaged over a designated area in Northeast Brazil from 0° S to 12.5° S and 37.5° W to 52° W. Model forecasts are compared with observational data taken from the NOAA/GPCP dataset (Adler et al. 2003). The comparison is made in terms of rainfall anomalies. The model rainfall anomaly is defined as the difference between a given year's FMA mean rainfall and the mean over all 39 forecasts. Note that this is different from just using a control experiment as in part 1, because the aggregate effect of all the different SSTAs will not add up to zero, even if the SSTAs do. As explained in part 1, the humidity flux arising from an SSTA is a nonlinear function of both the SSTA and the climatological SST, and the dynamical response of the

atmosphere is also nonlinear. It is also unlikely that the SSTAs will cancel exactly given the mismatch between the climatology and the forecast period, and any associated bias needs to be eliminated from the diagnosis.

In section 4 we evaluate the contributions of the Pacific, Atlantic and Indian Oceans to forecasts of Nordeste rainfall. The entire suite of ensemble forecasts is repeated using SSTAs restricted to individual ocean basins and disabling the effect of the SSTA elsewhere. This is possible without introducing extraneous bias because the control climate for DREAM does not depend on any SST data. The climatological effect of the sea surface is implicit in the empirical forcing. These restricted ocean basin forecasts are again evaluated relative to their mean over the 39 years of forecasts. In section 5 we further explore the sensitivity of the region to SSTs at all locations in the tropical band using a large array of artificial SSTAs in a set of experiments similar to those presented in part 1. Because these experiments use idealised SSTAs, the anomaly response is evaluated relative to a control run, as in part 1. Details of these artificial SSTAs, and how their influence can help simulate the forecast skill of the model are given in section 5.

3 | Model Validation and Seasonal Forecasts

Before looking at individual seasonal forecasts we first discuss the average behaviour of the forecast system across 39 years of January–May integrations with 38 different 1-Jan initial conditions defining the ensemble. Figure 1a shows the long-term mean FMA GPCP merged rainfall product we use as a reference. In part 1, this was compared with a 38-member FMA-mean ensemble mean from a control integration of DREAM, with no influence from SST anomalies (Figure 1b). In this article, we add the FMA-mean ensemble-mean forecast product, averaged over all 39 forecasts (Figure 1c,d).

The DREAM precipitation simulations reproduce the main features of the global observations, including the ITCZ and southern convergence zones. Tropical rainfall in DREAM is generally weaker than the observed rainfall and there are some differences in the placements of rainfall maxima. For example, the Atlantic ITCZ is too far south and the maximum over South America is too far north. The red rectangle on the figures denotes our reference area for Nordeste rainfall. Mean rainfall in this area will be used for forecast diagnostics in the rest of the article.

Comparing the control run with the forecast mean, they are almost identical, but there is a very slight drying in the forecasts on the eastern side of South America, consistent with our expectation from part 1 about the systematic effects of nonlinearity. The model bias is globally dry, but there is a complex distribution in the reference area owing to the misplaced continental rainfall maximum, and a weak secondary maximum to the southeast. The model systematic errors are generally within the bounds expected from a GCM.

Seasonal forecasts for each year from 1982 to 2020 will be expressed as departures from the forecast mean precipitation in

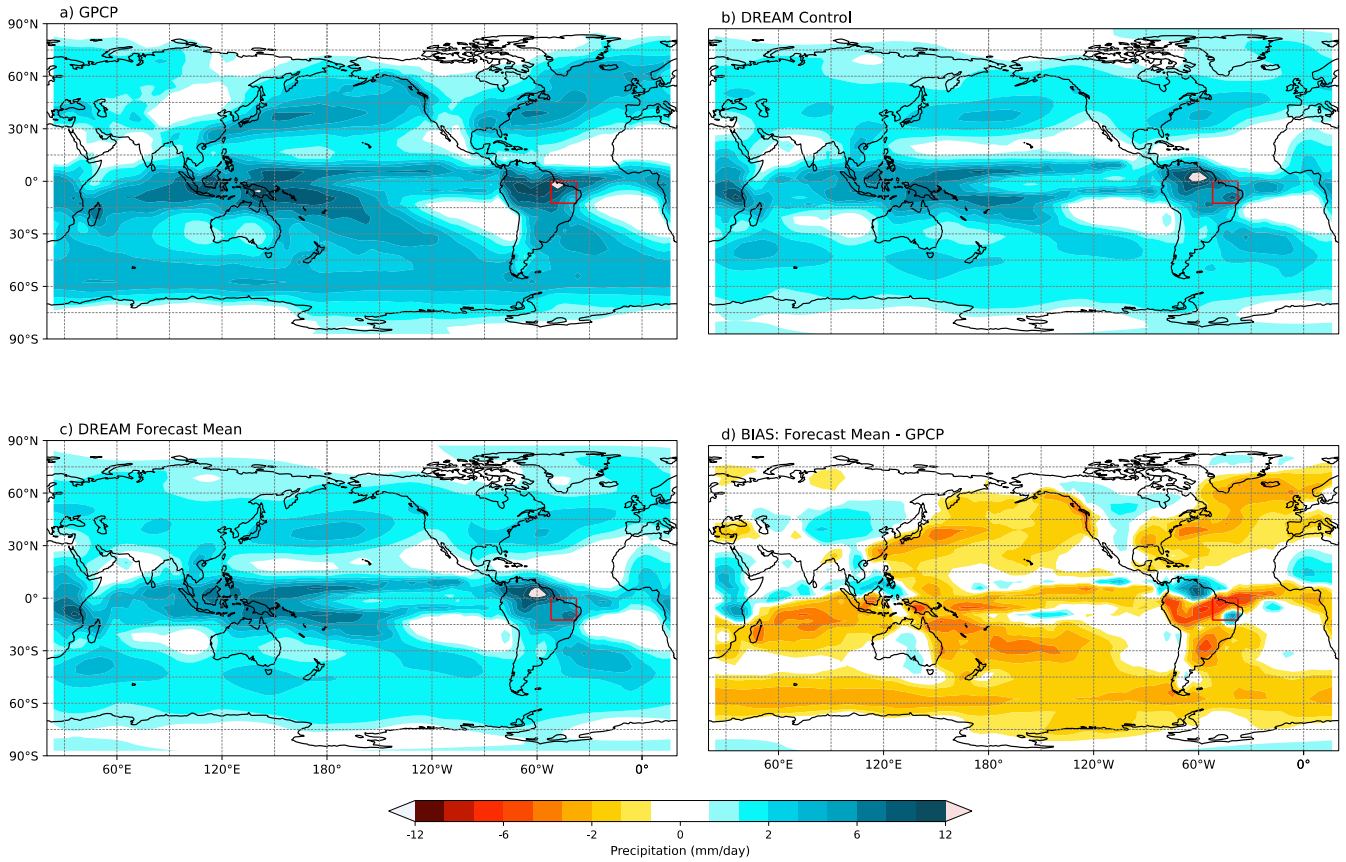

FIGURE 1 | FMA mean rainfall in mm/day for (a) GPCP climatology, (b) DREAM control ensemble mean, (c) DREAM forecast mean for the period 1982–2020, (d) DREAM systematic error (forecast mean minus GPCP). [Colour figure can be viewed at wileyonlinelibrary.com]

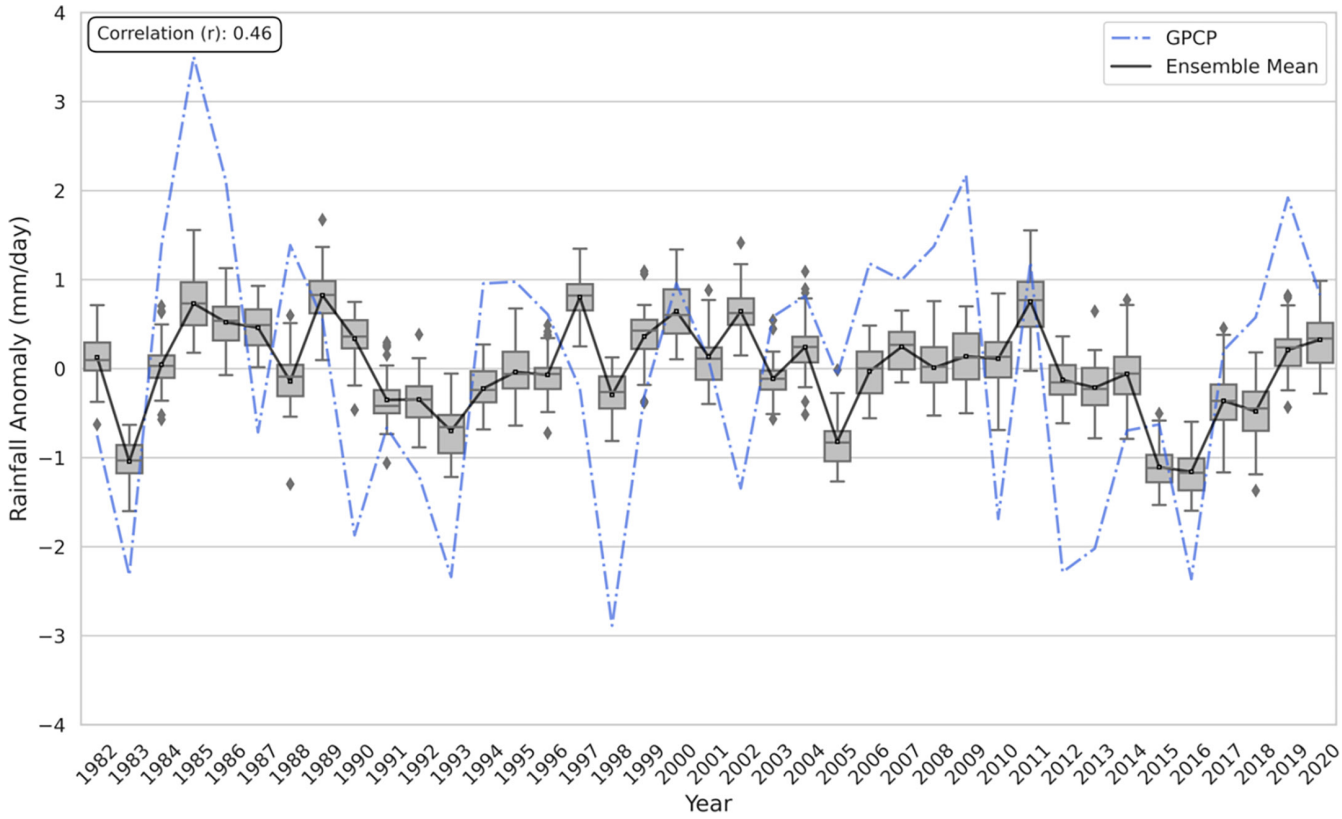

FIGURE 2 | FMA rainfall anomaly box plots for DREAM ensemble forecasts compared to GPCP anomalies. [Colour figure can be viewed at wileyonlinelibrary.com]

the reference area due to tropical SSTAs. Figure 2 shows box plots depicting the ensemble forecast for each year compared to the GPCP mean value. For each ensemble the box covers the interquartile range from the 25th to the 75th percentile and there is a bar inside the box at the median value. Bars outside the box then show maximum and minimum values that occur $<1.5\times$ the interquartile range outside the box, and outliers outside this range are marked with diamonds. A solid line joins the ensemble means marked by small open circles.

We can immediately see that the model has some interannual variability, but it is not as strong as in the observations. This is possibly due to the idealised nature of the model and experiments, in which the only source of interannual variation in the forcing is the tropical SSTAs. The spread of the ensemble each year is smaller than the interannual variability, although not by a large factor. This encourages us to believe that the SSTAs have a systematic influence on the model and that the ensemble mean might provide a useful forecast product. The spread of the ensembles is also quite variable in its own right, although there is no indication that narrower spreads align with better forecasts.

The key question now is how well does the ensemble mean do over the 39 years. Statistical information about the variability in ensemble mean forecast anomalies is summarised in a Taylor diagram in Figure 3, using GPCP as the reference. DREAM (black circle) and ECHAM (black square) are seen to have similar correlation coefficients (0.46 and 0.55, respectively) and similar RMS error, but as mentioned earlier, DREAM has weaker variability. NMME showed the best correlation among the results with a value of 0.72, however it showed a standard deviation value that was further away from the observation when compared with the ECHAM result. This can be explained by the fact that the NMME data is the average of the ensemble of models, which adds value to the skill and reduces variability. The DREAM correlation can be compared with a measure of the best that can be expected from the model, that is, how good is the model ensemble mean at predicting an given deterministic forecast? The interannual correlation between the ensemble mean and individual ensemble members ranges from 0.808 to 0.931. This puts the model ensemble mean forecast correlation of 0.46 in perspective, but also clearly indicates that there is much room for improvement.

A practical test of the forecast utility is its ability to predict wet and dry years. Table 1 gives contingencies based on terciles of wet, normal and dry events. Over the 39 years there are 13 in each category, so a perfect set of forecasts would place 13 s on the leading diagonal of the table and zeros elsewhere. DREAM is far from this ideal, but a brief perusal of Table 1 at least confirms that the model gets wet and dry years right at least twice as often as it gets them wrong.

Table 1 can be used to generate a wide variety of skill scores. If the analysis is limited to wet and dry years, the mean of the two resulting F1 scores for DREAM is 0.687 and for ECHAM it is 0.833. So in general the forecast performance of DREAM

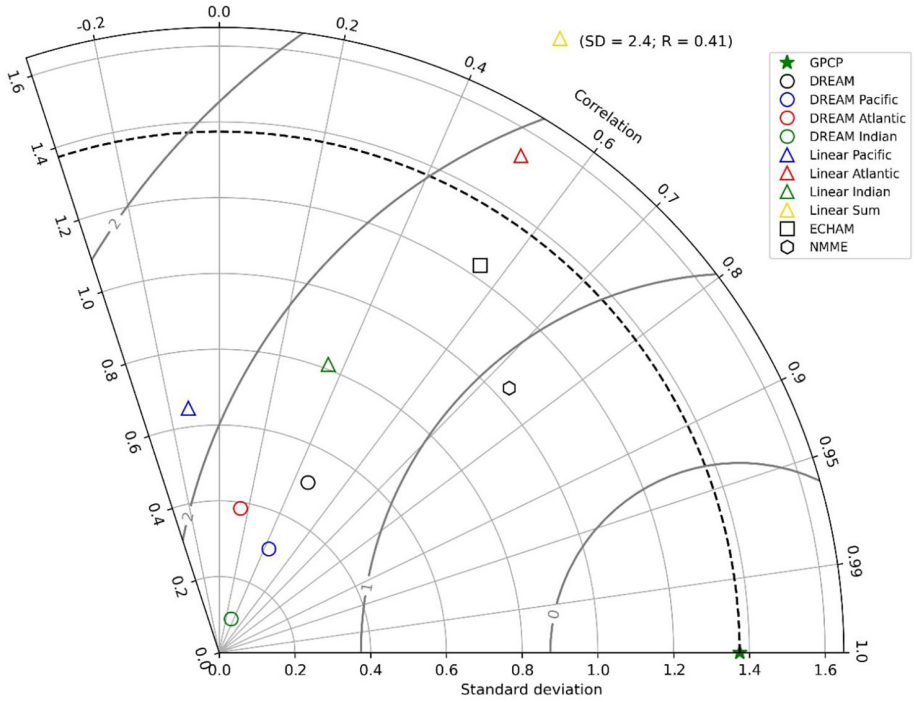

FIGURE 3 | Taylor diagram for interannual variability of FMA forecast ensemble means (DREAM, ECHAM and NMME) and linear calculations, referenced to GPCP anomalies. Correlation is angular distance, standard deviation is radial distance, RMSE is direct distance (grey circles). [Colour figure can be viewed at wileyonlinelibrary.com]

TABLE 1 | Contingencies of wet, normal and dry years predicted by DREAM (and by forecasts generated from individual ocean basin SSTAs in parentheses) and by ECHAM.

		DREAM (Pac, Atl, Ind, Sum) ECHAM		
		Dry	**Normal**	**Wet**
Verification	Dry	6 (4,5,3,6) 8	4 (6,4,8,4) 4	3 (3,4,2,3) 1
	Normal	5 (6,5,7,5) 3	3 (3,4,1,3) 5	5 (4,4,5,5) 5
	Wet	2 (3,3,3,2) 2	6 (4,5,4,6) 4	5 (6,5,6,5) 7

could be described as respectable but it falls short of the fully specified GCM.

A more exacting test for the model (Van den Dool and Toth 1991) is obtained when we consider all three classes: wet, normal and dry. Respectively for each of these classes, the F1 scores for DREAM are 0.38, 0.23 and 0.46. The corresponding scores for ECHAM are 0.53, 0.38 and 0.61. We naturally expect lower scores in a three-category system, but it appears that although DREAM does a reasonable job differentiating wet from dry, it has much more difficulty identifying years where the rainfall is outside the middle tercile. The ECHAM model also presents its weakest skill in identifying normal years, but it has a more consistent performance than DREAM. These scores are in line with what we would expect from a direct examination of the contingency matrix shown in Table 1.

Since our focus in this article is not on presenting a forecast product, but on testing and understanding it, we will not dwell any further on performance statistics, but proceed to some diagnostics to investigate the physical basis of this forecast performance.

4 | Attribution of Forecast Performance to Different Ocean Basins

In part 1 we examined the separate and combined influences of fixed SSTA patterns in the Pacific and the Atlantic. The broad conclusion was that their influence in Nordeste rainfall is additive and that the larger SSTAs in the Pacific lead to a predominant Pacific signal. Do these conclusions carry through to an assessment of forecast performance? To answer this question the entire suite of hindcasts was rerun three times, retaining only the SSTAs from the Pacific, Atlantic and Indian Oceans in turn. The results are shown in Figure 4 as the difference between the yearly ensemble mean and the forecast mean. The forecast mean was evaluated separately for each experiment to make sure that the anomaly arises only from SSTAs, and not from any systematic difference between an experiment forced from a single ocean basin and an experiment forced from the entire tropics.

The Pacific Ocean timeseries looks quite similar to the main forecast and correlates almost as well at $r = 0.43$. It is, however lacking in variability, indicating that although the Pacific is

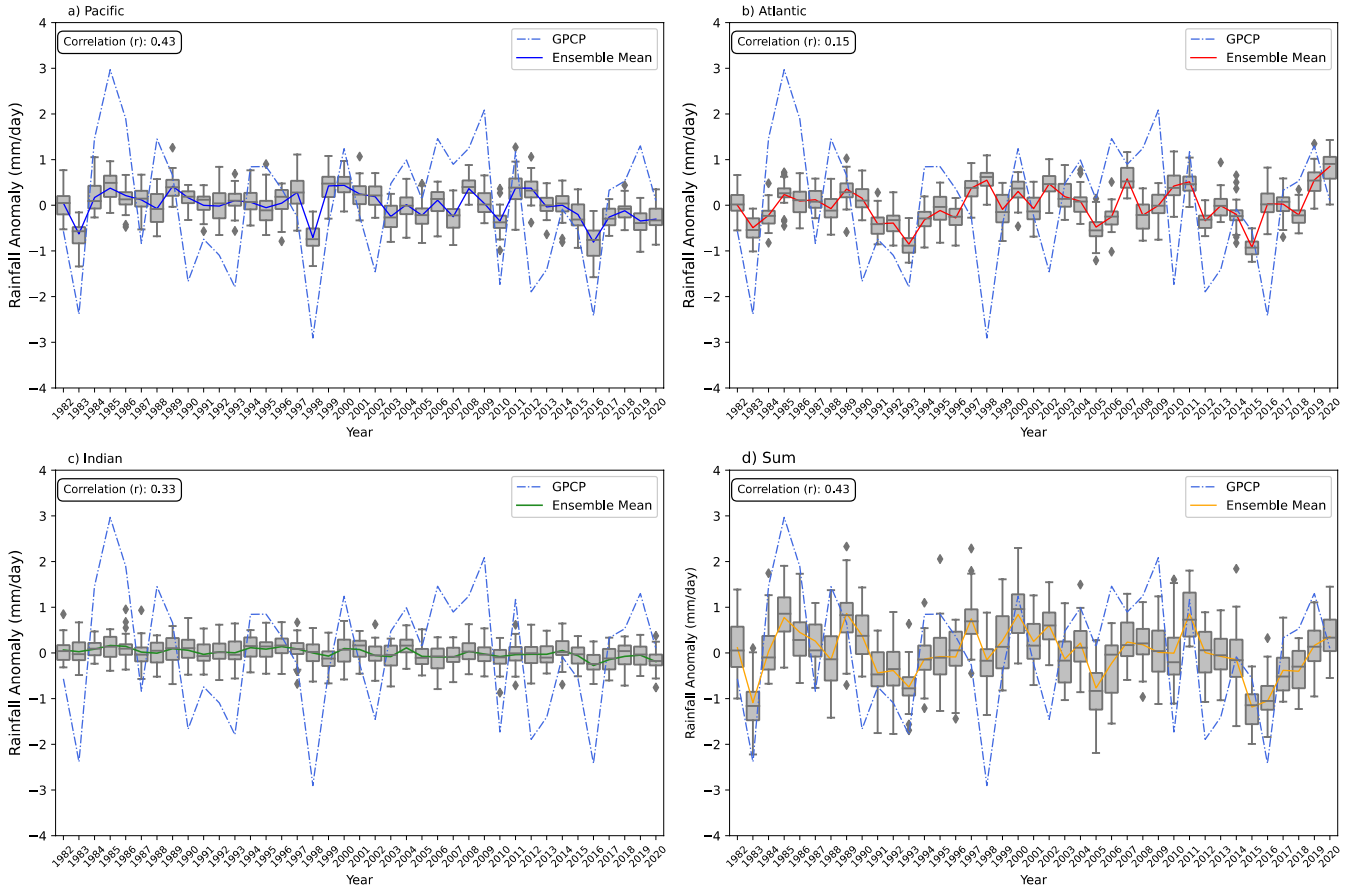

FIGURE 4 | Box plots as in Figure 2 for individual ocean basin ensemble forecast runs, (a) Pacific, (b) Atlantic, (c) Indian Ocean and (d) the sum of the three. [Colour figure can be viewed at wileyonlinelibrary.com]

not the only influence, it may well be the most useful influence in terms of forecast skill. Nevertheless, its performance in terms of predicting wet and dry years is slightly worse (Table 1). The Atlantic actually furnishes more interannual variability than the Pacific, but little of it contributes to forecast performance and the correlation is only 0.15. Information from the Atlantic is quite indiscriminate in terms of wet and dry years. Variability attributable to the Indian Ocean is very weak indeed. Every forecast is within the ensemble range of every other forecast. The correlation coefficient for ensemble means is 0.33 but this has little meaning with such weak variability. The circles in Figure 3 summarise the statistics for the single ocean basin experiments. Outside the Nordeste target region, global distributions of rainfall temporal correlation (not shown) have generally low values with isolated maxima for the Atlantic and Indian Ocean runs. Only the Pacific run has substantial areas of high correlation, and that is mostly over the ocean. The strong influence of El Niño, and in particular extreme eastern Pacific El Niños via teleconnections has been noted in previous GCM studies (see e.g., Kim, Kryjov, and Ahn 2022; Beniche et al. 2024).

Do our mostly linear predictions from part 1 mean that the characteristics of the full forecast can be recovered from the sum of these three runs? This appears to be the case, as the resulting curve follows the full forecast curve quite closely (compare Figure 4d with Figure 2). The correlation coefficient for the sum is 0.43 and the exact same values are recovered for the contingency table. Note that the ensemble spread for the sum of the three ocean basins is greater than the spread for the full tropical forecast. This is possible if the ensemble members for the three separate forecasts are correlated, presumably due to their shared initial conditions. So even though the ensemble mean is independent of the initial conditions, for each ensemble member the initial condition does appear to have a systematic effect.

5 | Influence Functions for Global SSTs and a Linear Forecast Simulation

In this section we extend the idea of attributing the Nordeste rainfall anomaly to remote sources, as we attempt to break it down still further to sub-basin scale SSTAs. To set the scene, consider the observed interannual covariance statistics between the study area and tropical SSTAs. This is presented in three ways in Figure 5. The correlation coefficient (Figure 5a) is a measure of the interannual relationship between a regional index and a global SSTA field, plotted as a global map of a dimensionless quantity. A regression is then presented in Figure 5b as a measure of sensitivity: the covariance normalised by the variance of the precipitation anomaly, plotted as a global map of SSTA in°C per mm/day, that is, the SSTA amplitude required for a given rainfall anomaly. Note that equatorial Pacific SSTAs stand out in this plot because the Nordeste region is relatively insensitive, so a large SSTA is required. Therefore, high

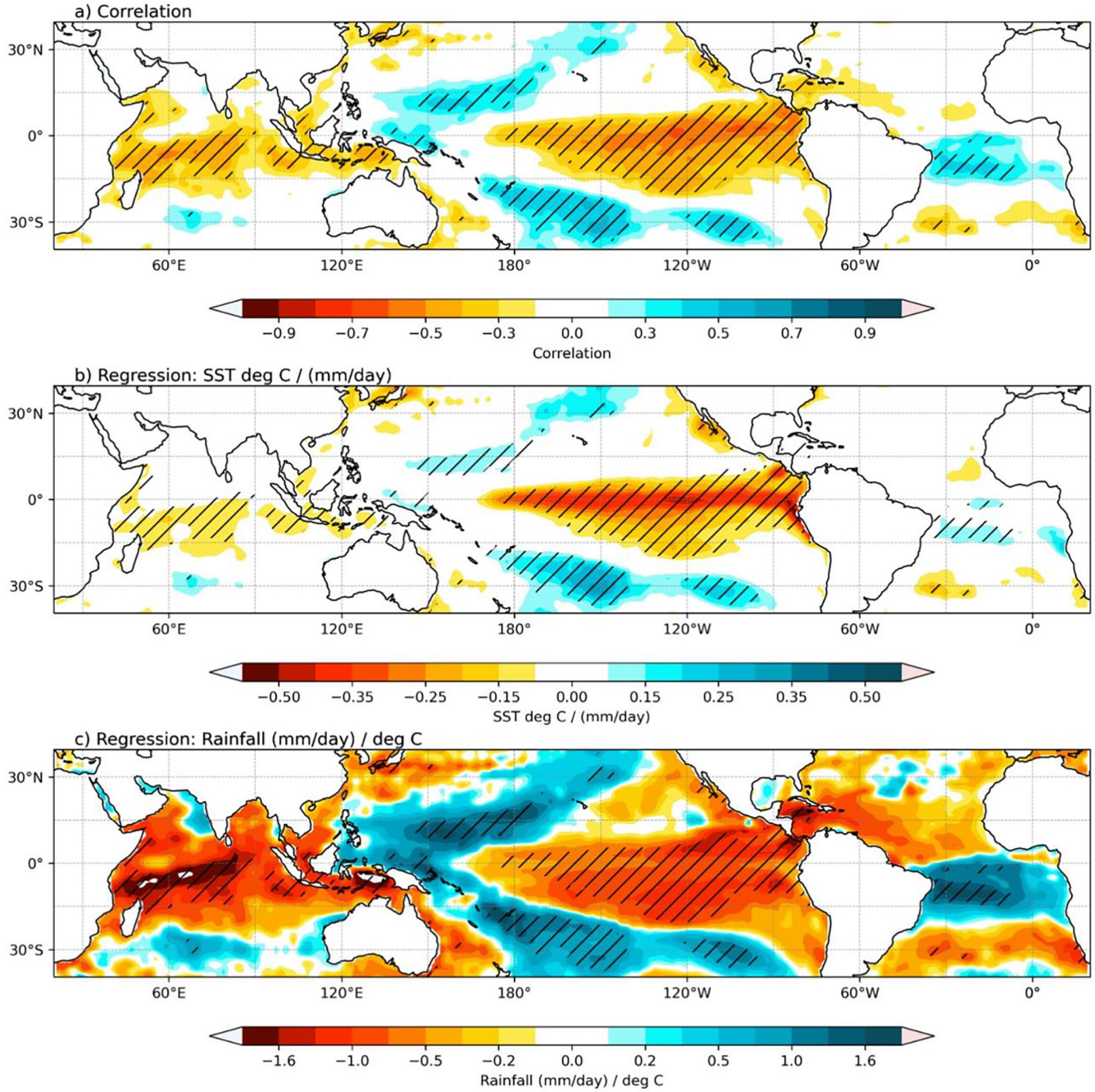

FIGURE 5 | Covariance statistics for GPCP rainfall anomalies in northestern Brazil (red box) and global Reynolds SSTA: (a) Correlation (dimensionless); (b) sensitivity regression (°C SSTA per mm/day); (c) response regression (mm/day per°C SSTA). Hatching areas indicates significant correlation at 5% significance level using *t*-test. [Colour figure can be viewed at wileyonlinelibrary.com]

correlations observed in the Pacific are due to the very large amplitude anomalies typically present in this region. An alternative regression is presented in a third way in Figure 5c as a measure of response. This time the covariance is normalised by the variance of the SSTA in situ. It is plotted as a global map of Nordeste rainfall in the position of the associated SSTA. So, every point on the global map actually shows values of rainfall in the target region. The units are mm/day per°C, that is, the rainfall response for a given SSTA. The distribution looks quite different, emphasising the sensitivity of the region to Atlantic SSTAs. Note that these three plots are not the same, because the normalising factor for SSTA is spatially distributed and appears at different degrees in the denominator each time. It should also be stressed that these plots cannot be used immediately for attribution. Data for SSTAs is not independent either regionally or even from one ocean basin to another.

It would be interesting to recast Figure 5c in a framework where it actually represents causality and can therefore be used for attribution and forecasting. This is possible if we use the model. A large number of independent perturbation experiments have been carried out with DREAM, in the same ensemble forecast

configuration as above (and also in part 1), but with an array of fixed artificial SSTAs of 1°C on a regular grid around the tropics. One SSTA covers a square region of side length 11.25° encompassing nine model grid points. Four latitude rows are considered and 32 longitudes, for a total of 128 ensemble forecast runs. Figure 6 shows an example of a single run, with an SSTA in the mid-Pacific (blue square). The FMA ensemble mean precipitation anomaly is plotted. There is a large direct response to the SSTA which excites upward motion to the west and downward to the east. The perturbation produces global teleconnections with a dry anomaly over the target region (red box).

Positions for the other SSTAs are shown as blue crosses. In Figure 7 the FMA ensemble mean precipitation anomaly averaged in the red box for each of these experiments is plotted at the position of the SSTA. This figure is an influence function. It summarises the behaviour of DREAM for Nordeste rainfall as a consequence of tropical SSTAs. It is natural to compare this figure with the 'response' regression shown in Figure 5c. The fundamental difference between the two figures is that the influence function actually shows causality, not just covariance, albeit in the framework of an imperfect model.

Some of the same broad characteristics are reproduced in the model result, including the predominance of the Atlantic as a strong influence per unit SSTA and the change in sign of the tropical Atlantic influence across the equator. There are also important differences, such as the east–west distribution of North Atlantic influence and the missing wet influence from the far western Pacific. These discrepancies may in part be due to model error, but there is likely to be a strong effect from the non-independence of the SST data in the regression.

Having established the influence function for this particular type of forecast run and forecast metric, we are now in a position to reconstruct the entire sequence of seasonal forecasts presented in sections 3 and 4, assuming that the response of DREAM to these isolated artificial SSTAs can be scaled and combined in a linear fashion. An FMA forecast for a given year's Nordeste rainfall anomaly with persisted tropical SSTAs can be immediately calculated by multiplying the January SSTA with the influence function and then summing the 128 separate contributions. The degraded resolution of the influence function was handled by simply applying the same value in the 9×9 grid box and multiplying it by full resolution January SSTAs with land values set to zero, averaging for each box and summing over all 128 boxes. This sum can be partitioned directly into contributions from the three ocean basins. The result is a linear model of the behaviour of DREAM, shown in Figure 8 for all 39 forecast years.

Figure 8a shows time series for the linear model compared with DREAM and the GPCP rainfall data. The DREAM results shown in Figure 4 for the three ocean basins are plotted together in Figure 8b (note the different scale), illustrating the close match between their sum and the full tropical experiment. Equivalent plots for the linear model are then shown in Figure 8c. In this case the sum is formally identical to the tropical band result shown in Figure 8a. The time variance statistics for the linear model are shown as triangles in the Taylor diagram in Figure 3.

The interannual variance of the linear model is much greater than for DREAM and is in fact unrealistically large compared with the observations. On the other hand, the correlation is similar. However, the linear model curve is not just an amplified version of the DREAM curve, as it fluctuates from year to year with large amplitude. Linear simulations of the individual ocean contributions also differ from the DREAM results. The Atlantic contribution is stronger than the Pacific for the linear calculations, and the Atlantic now correlates well with GPCP, whereas the Pacific actually has a small negative correlation. So, the fact

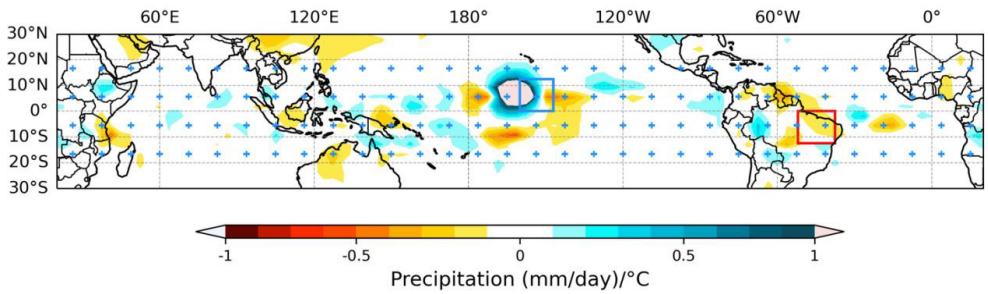

FIGURE 6 | A single example of an idealised run showing ensemble mean FMA precipitation anomaly (mm/day) from an SSTA in the mid-Pacific (blue square). SSTA centres for all 128 idealised experiments are shown as blue crosses. [Colour figure can be viewed at wileyonlinelibrary.com]

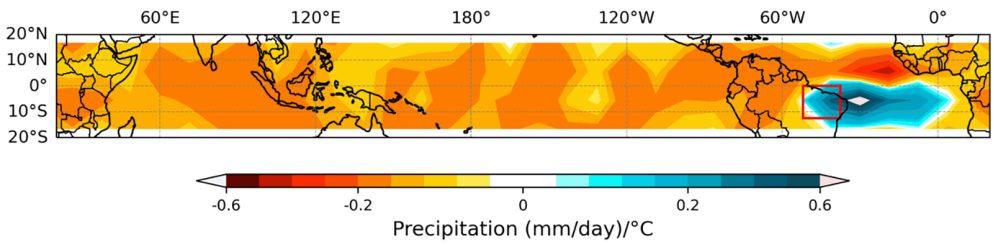

FIGURE 7 | Influence function for mean rainfall (mm/day) in the red box, plotted in the location of the idealised SSTA that caused it. [Colour figure can be viewed at wileyonlinelibrary.com]

FIGURE 8 | Linear hindcast experiments compared with DREAM: (a) Full tropical SSTA DREAM forecasts, the linear result and the GPCP reference, (b) DREAM runs for individual ocean basins plus their sum and the full tropical run (note the reduced scale); (c) Linear results for the individual ocean basins and their sum. [Colour figure can be viewed at wileyonlinelibrary.com]

that DREAM and the linear sum have similar correlations with GPCP is largely fortuitous, arising from different contributions from the Atlantic and Pacific. In both cases the Indian Ocean contributes very little. We can tentatively conclude that combinations of influences from the Atlantic interfere destructively in DREAM, and perhaps the opposite is true for the Pacific.

6 | Discussion

This article is the second part of an extended test of a novel global modelling system applied to the interannual variability of rainfall over South America. Part 1 provided an academic study of canonical SST anomalies, and their impact in ensemble forecast experiments. Here in part 2 this is extended to real interannual SST anomalies and an evaluation of forecast performance for a specified region of Northeast Brazil over a 39-year period.

Some of the conclusions from part 1 carry over into this more applied forecasting context. The model has a reasonably good response to well-known SSTA patterns, and this translates to a reasonably good performance in year-by-year seasonal forecasting. The additive nature of the response to combined canonical patterns found in part 1 is also reflected in the way individual ocean basins contribute to the seasonal forecast.

However, this straightforward additive character did not endure for smaller-scale SST anomalies, and some intriguing differences arose between the full DREAM forecasts and the linear calculations based on the influence function. The low interannual variance of DREAM stands in contrast with the linear results, and the origins of forecast skill are also quite different. It seems that DREAM is not sensitive enough to the influence of the entire Atlantic, but more sensitive to smaller SSTAs within the Atlantic. To some extent the opposite effect is observed in the Pacific. This warrants further investigation, and more idealised studies could be conceived to look at the relationship between the nonlinearity of the impact, and the scale and location of the SSTA. A further complicating factor may arise from the difference in persistence of SSTAs between the Atlantic and the Pacific. Atlantic SSTAs typically develop more during a forecast, reducing the value of the persisted SSTA. Experiments in which the SSTA develops during the forecast can easily be carried out with DREAM to evaluate this effect. In fact, it will be interesting to evaluate the contribution that SSTA development can make to forecast skill not only for the Nordeste region considered in this work but for other regions and other rainy seasons where it may be of greater importance.

It is worth commenting on the scope of applicability of DREAM. It can be viewed as an economical option for seasonal forecasting. An alternative would be to consult the freely available NMME product (Kirtman et al. 2014) generated from a super-ensemble of GCM forecasts. For the specific region and season considered in this article, the performance of NMME is similar to the ECHAM forecasts carried out at FUNCEME (better correlation worser variability). Another alternative would be to rely on statistical models, which in some locations may offer similar skill in situations that are analogous to past events. However, the use of DREAM confers some advantages. It offers rapid access to physical interpretation and the flexibility of supplementary experiments at a reduced cost that may be useful for forecasters. Such experiments could be deployed as a quick test, to be repeated with an in-house GCM, or as an alternative to an in-house GCM for those that rely entirely on freely available community products such as NMME.

DREAM is already in place at FUNCEME as an operational model and has been used to forecast the Nordeste rainy season from 2022 to 2024. At this point, we have concentrated almost exclusively on this region but the global rainfall climatology of DREAM seems realistic enough to envisage extensions to this work. There is ample scope to use DREAM in other parts of the world, for other rainy seasons, where it might potentially have a place as an economical option for hybrid research and forecasting activities, particularly where computer resources are limited.

Author Contributions

Francisco das Chagas Vasconcelos Junior: investigation, methodology, visualization, writing – review and editing, software, formal analysis. **Nicholas M. J. Hall:** conceptualization, investigation, writing – original draft, validation, writing – review and editing, formal analysis, methodology, supervision, resources, software. **Leticia Cardoso:** writing – review and editing, visualization, software. **Aubains Hounsou-Gbo:** conceptualization, investigation, software. **Eduardo S. P. R. Martins:** investigation, formal analysis, supervision, project administration, writing – review and editing.

Acknowledgements

FVJ Thanks to the National Council for Scientific and Technological Development (CNPq) with processes numbers 409666/2021-1 and 16867/2023-3. NH, AH, FVJ, LC and EM thanks to 'Institut de recherche pour le développement (IRD)' for supporting the International Research Network CARDAPIO. NH was supported by IRD (Institut de Recherche pour le Developpement) during a sabbatical at Funceme. We thank to the National Oceanic and Atmospheric Administration (NOAA) for providing the precipitation dataset GPCP (https://psl.noaa.gov/data/gridded/data.gpcp.html) and the SST dataset from Optimum Interpolation SST (https://psl.noaa.gov/data/gridded/data.noaa.oisst.v2.html). We thank the reviewers for pertinent remarks that led to a clearer and more complete account of our work.

Conflicts of Interest

The authors declare no conflicts of interest.

Data Availability Statement

Data will be made available on request.

References

Adler, R. F., G. J. Huffman, A. Chang, et al. 2003. "The Version-2 Global Precipitation Climatology Project (GPCP) Monthly Precipitation Analysis (1979–Present)." *Journal of Hydrometeorology* 4, no. 6: 1147–1167.

Balmaseda, M., D. L. T. Anderson, and M. K. Davey. 1994. "ENSO Prediction Using a Dynamical Ocean Model Coupled to Statistical Atmospheres." *Tellus A* 46, no. 4: 497–511.

Barnett, T. P., and R. Preisendorfer. 1987. "Origins and Levels of Monthly and Seasonal Forecast Skill for United States Surface Air Temperatures Determined by Canonical Correlation Analysis." *Monthly Weather Review* 115: 1825–1850.

Barnett, T. P., M. Latif, N. Graham, M. Flugel, S. Pazane, and W. White. 1993. "ENSO and ENSO Related Predictability. I: Prediction of Equatorial Pacific Sea Surface Temperature With a Hybrid Coupled Ocean-Atmosphere Model." *Journal of Climate* 6: 1545–1566.

Barnston, A. G., S. J. Mason, L. Goddard, D. G. DeWitt, and S. E. Zebiak. 2003. "Multimodel Ensembling in Seasonal Climate Forecasting at IRI." *Bulletin of the American Meteorological Society* 84, no. 12: 1783–1796.

Basso, B., and L. Liu. 2019. "Seasonal Crop Yield Forecast: Methods, Applications, and Accuracies." *Advances in Agronomy* 154: 201–255.

Beniche, M., J. Vialard, M. Lengaigne, A. Voldoire, G. Srinivas, and N. M. Hall. 2024. "A Distinct and Reproducible Teleconnection Pattern Over North America During Extreme El Niño Events." *Scientific Reports* 14, no. 1: 2457.

Cai, W., M. J. McPhaden, A. M. Grimm, et al. 2020. "Climate Impacts of the El Niño–Southern Oscillation on South America." *Nature Reviews Earth and Environment* 1, no. 4: 215–231.

Canamary, E., D. Reis Jr., and E. Martins. 2015. "Evaluation of Ensemble SPI Forecasts for Ceará, Northeastern Brazil." In *Drought: Research and Science-Policy Interfacing*, 1st ed., 245. Boca Raton: CRC Press.

Coelho, C. A., D. C. de Souza, P. Y. Kubota, et al. 2021. "Evaluation of Climate Simulations Produced With the Brazilian Global Atmospheric Model Version 1.2." *Climate Dynamics* 56: 873–898.

Delgado, J. M., S. Voss, G. Bürger, et al. 2018. "Seasonal Drought Prediction for Semiarid Northeastern Brazil: Verification of Six Hydro-Meteorological Forecast Products." *Hydrology and Earth System Sciences* 22, no. 9: 5041–5056.

Derome, J., H. Lin, and G. Brunet. 2005. "Seasonal Forecasting With a Simple General Circulation Model: Predictive Skill in the AO and PNA." *Journal of Climate* 18, no. 4: 597–609.

Dirmeyer, P. A., and S. Halder. 2017. "Application of the Land–Atmosphere Coupling Paradigm to the Operational Coupled Forecast System, Version 2 (CFSv2)." *Journal of Hydrometeorology* 18, no. 1: 85–108.

Doblas-Reyes, F. J., J. García-Serrano, F. Lienert, A. P. Biescas, and L. R. L. Rodrigues. 2013. "Seasonal Climate Predictability and Forecasting: Status and Prospects." *WIREs Climate Change* 4: 245–268. https://doi.org/10.1002/wcc.217.

Eade, R., D. Smith, A. Scaife, et al. 2014. "Do Seasonal-to-Decadal Climate Predictions Underestimate the Predictability of the Real World?" *Geophysical Research Letters* 41, no. 15: 5620–5628.

Folland, C. K., A. W. Colman, D. P. Rowell, and M. K. Davey. 2001. "Predictability of Northeast Brazil Rainfall and Real-Time Forecast Skill, 1987–98." *Journal of Climate* 14: 1937–1958. https://doi.org/10.1175/1520-0442(2001)014<1937:PONBRA>2.0.CO;2.

Hagedorn, R., F. J. Doblas-Reyes, and T. N. Palmer. 2005. "The Rationale Behind the Success of Multi-Model Ensembles in Seasonal Forecasting-II." *Calibration and Combination, Tellus A* 57: 234–252.

Hall, N. M. J. 2000. "A Simple GCM Based on Dry Dynamics and Constant Forcing." *Journal of the Atmospheric Sciences* 57: 1557–1572.

Hall, N. M. J., and S. Leroux. 2023. "Dream User Manual v8.4." Zenodo. https://doi.org/10.5281/zenodo.8414525.

Hall, N. M. J., S. Leroux, and T. Ambrizzi. 2019. "Transient Contributions to the Forcing of the Atmospheric Annual Cycle: A Diagnostic Study With the DREAM Model." *Climate Dynamics* 52, no. 11: 6719–6733.

Hall, N. M. J., H. Lin, and J. Derome. 2001. "The Extratropical Signal Generated by a Midlatitude SST Anomaly. Part II: Influence on Seasonal Forecasts." *Journal of Climate* 14, no. 12: 2696–2709.

Hastenrath, S. 2012. "Exploring the Climate Problems of Brazil's Nordeste: A Review." *Climatic Change* 112, no. 2: 243–251.

Hoskins, B. 2013. "The Potential for Skill Across the Range of the Seamless Weather-Climate Prediction Problem: A Stimulus for Our Science." *Quarterly Journal of the Royal Meteorological Society* 139, no. 672: 573–584.

Hoskins, B. J., and A. J. Simmons. 1975. "A Multi-Layer Spectral Model and the Semi-Implicit Method." *Quarterly Journal of the Royal Meteorological Society* 101, no. 429: 637–655.

Hounsou-Gbo, A., N. Hall, L. Cardoso, F. C. Vasconcelos Jr., and E. S. P. R. Martins. 2024. "Simple GCM Simulations of Rainfall Over Northeastern Brazil, Part 1: Systematic Effect of Canonical Sea Surface Temperature Patterns."

Kim, E. S., V. N. Kryjov, and J. B. Ahn. 2022. "Predictability of the Wintertime Western Pacific Pattern in the APEC Climate Center Multi-Model Ensemble." *Atmosphere* 13, no. 11: 1772.

Kirtman, B., and A. Pirani. 2009. "The State of the Art of Seasonal Prediction: Outcomes and Recommendations From the First World Climate Research Program Workshop on Seasonal Prediction." *Bulletin of the American Meteorological Society* 90, no. 4: 455–458. http://www.jstor.org/stable/26220969.

Kirtman, B. P., D. Min, J. M. Infanti, et al. 2014. "The North American Multi-Model Ensemble (NMME): Phase-1 Seasonal to Interannual Prediction, Phase-2 Toward Developing Intra-Seasonal Prediction." *Bulletin of the American Meteorological Society* 95: 585–601. https://doi.org/10.1175/BAMS-D-12-00050.1.

Li, H., L. Luo, E. F. Wood, and J. Schaake. 2009. "The Role of Initial Conditions and Forcing Uncertainties in Seasonal Hydrologic Forecasting." *Journal of Geophysical Research: Atmospheres* 114, no. D4.

Mason, S. J., L. Goddard, N. E. Graham, E. Yulaeva, L. Sun, and P. A. Arkin. 1999. "The IRI Seasonal Climate Prediction System." In *WRPMD'99: Preparing for the 21st Century*, 1–5.

Misra, V. 2006. "Understanding the Predictability of Seasonal Precipitation Over Northeast Brazil." *Tellus A: Dynamic Meteorology and Oceanography* 58, no. 3: 307–319. https://doi.org/10.1111/j.1600-0870.2006.00175.x.

Moron, V., and A. W. Robertson. 2020. "Tropical Rainfall Subseasonal-to-Seasonal Predictability Types." *NPJ Climate and Atmospheric Science* 3, no. 1: 4.

Pereira, J. M. R., C. D. C. Raimundo, D. S. Reis Jr., F. D. C. Vasconcelos Jr., and E. S. P. R. Martins. 2023. "Use of Climate Information in Water Allocation: A Case of Study in a Semiarid Region." *Watermark* 15: 2460. https://doi.org/10.3390/w15132460.

Pilz, T., J. M. Delgado, S. Voss, et al. 2019. "Seasonal Drought Prediction for Semiarid Northeast Brazil: What Is the Added Value of a Process-Based Hydrological Model?" *Hydrology and Earth System Sciences* 23, no. 4: 1951–1971.

Reynolds, R. W., N. A. Rayner, T. M. Smith, D. C. Stokes, and W. Wang. 2002. "An Improved In Situ and Satellite SST Analysis for Climate." *Journal of Climate* 15, no. 13: 1609–1625.

Roads, J. O. 1987. "Predictability in the Extended Range." *Journal of the Atmospheric Sciences* 44: 3495–3527.

Robertson, A., and F. Vitart. 2018. *Sub-Seasonal to Seasonal Prediction: The Gap Between Weather and Climate Forecasting*. Amsterdam, The Netherlands: Elsevier.

Roeckner, E., K. Arpe, L. Bengtsson, et al. 1996. The Atmospheric General Circulation Model ECHAM-4: Model Description and Simulation of Present-Day Climate Max-Planck Institute for Meteorology, Report No. 218, Hamburg, Germany, 90 pp.

Ropelewski, C. F., and M. S. Halpert. 1987. "Global and Regional Scale Precipitation Patterns Associated With the El Niño/Southern Oscillation." *Monthly Weather Review* 115, no. 8: 1606–1626.

Scaife, A. A., L. Ferranti, O. Alves, et al. 2019. "Tropical Rainfall Predictions From Multiple Seasonal Forecast Systems." *International Journal of Climatology* 39, no. 2: 974–988.

Shukla, S., A. McNally, G. Husak, and C. Funk. 2014. "A Seasonal Agricultural Drought Forecast System for Food-Insecure Regions of East Africa." *Hydrology and Earth System Sciences* 18, no. 10: 3907–3921.

Simmons, A. J. 2006. "ERA-Interim: New ECMWF Reanalysis Product From 1989 Onwards." *ECMWF Newsletter* 110: 25.

Stevens, B., M. Giorgetta, M. Esch, et al. 2013. "Atmospheric Component of the MPI-M Earth System Model: ECHAM6." *Journal of Advances in Modeling Earth Systems* 5, no. 2: 146–172.

Tang, Y., H. Lin, and A. M. Moore. 2008. "Measuring the Potential Predictability of Ensemble Climate Predictions." *Journal of Geophysical Research: Atmospheres* 113, no. D4: 1–23.

Tompkins, A. M., M. I. O. De Zárate, R. I. Saurral, et al. 2017. "The Climate-System Historical Forecast Project: Providing Open Access to Seasonal Forecast Ensembles From Centers Around the Globe." *Bulletin of the American Meteorological Society* 98, no. 11: 2293–2301.

Uvo, C. B., C. A. Repelli, S. E. Zebiak, and Y. Kushnir. 1998. "The Relationships Between Tropical Pacific and Atlantic SST and Northeast Brazil Monthly Precipitation." *Journal of Climate* 11: 551–562. https://doi.org/10.1175/1520-0442(1998)011<0551:TRBTPA>2.0.CO;2.

Van Den Dool, H. M., and Z. Toth. 1991. "Why Do Forecasts for "Near Normal" Often Fail?" *Weather and Forecasting* 6, no. 1: 76–85.

Vasconcelos Junior, F. C., C. Jones, A. W. Gandu, and E. S. P. Martins. 2021. "Impacts of the Madden-Julian Oscillation on the Intensity and Spatial Extent of Heavy Precipitation Events in Northern Northeast Brazil." *International Journal of Climatology* 41, no. 6: 3628–3639.

Ward, M. N., and C. K. Folland. 1991. "Prediction of Seasonal Rainfall in North Nordeste of Brazil Using Eigenvectors of SST." *International Journal of Climatology* 11: 711–744.